Differential Nonlinear Robustness of Critical States in Fibonacci and Tribonacci Substitution Chains

A Numerical Study of Discrete Nonlinear Schrödinger Dynamics

Pablo Nogueira Grossi
G6 LLC, Newark, New Jersey, USA
ORCID: 0009-0000-6496-2186
pablogrossi@hotmail.com

Zenodo: 10.5281/zenodo.20026943

May 2026

Abstract

We study the discrete nonlinear Schrödinger (DNLS) equation on two quasiperiodic tight-binding chains: the Fibonacci chain ($n = 2$) and the Rauzy–tribonacci chain ($n = 3$), generated by their respective substitution rules. Starting from mid-gap eigenstates of the linear Hamiltonian, we integrate the DNLS time evolution over a range of nonlinearity strengths $\lambda \in [0, 10]$ and track the inverse participation ratio (IPR) as a measure of localization. The tribonacci chain exhibits a mid-gap IPR approximately four times larger than the Fibonacci chain in the linear limit, consistent with the stronger multifractality of Rauzy fractal eigenstates. Under nonlinear perturbation, the Fibonacci mid-gap state delocalizes rapidly (IPR drops $\sim 60\%$ at $\lambda = 1.5$), while the tribonacci state remains nearly pinned (IPR drop $< 5\%$ at the same coupling). We term this *differential nonlinear robustness*: the tribonacci chain's more strongly multifractal spectrum provides greater effective resistance to nonlinear delocalization. The characteristic decay constant of the tribonacci amplitude envelope, $\eta \approx 1.839287$, is the Perron–Frobenius eigenvalue of the tribonacci companion matrix, whose existence and key properties ($\eta > 1$, strict antitonicity of η^{-k}) are formally verified in Lean 4/Mathlib4 in the companion AXLE repository [21]. Our results constitute, to our knowledge, the first numerical study of DNLS dynamics on a tribonacci substitution chain, and identify a qualitative difference in nonlinear response between $n = 2$ and $n = 3$ substitution-generated quasicrystal models.

Keywords: tribonacci chain; Fibonacci quasicrystal; discrete nonlinear Schrödinger equation; multifractality; inverse participation ratio; Rauzy substitution; nonlinear localization; quasiperiodic tight-binding

1 Introduction

Quasiperiodic tight-binding chains generated by substitution rules have been a canonical setting for studying the interplay between long-range order, multifractality, and localization since the 1980s. The Fibonacci chain—the $n = 2$ case of the n-bonacci family—occupies a central role: its spectrum is a Cantor set of measure zero, its eigenstates are critical (neither extended nor localized), and their multifractal dimensions are precisely computable [1–4]. Topological phases, charge pumping, and one-dimensional quasicrystalline superconductivity have been analyzed in the Fibonacci setting [5, 6].

The natural generalization to tribonacci and higher n-bonacci substitution chains is more recent. Krebbekx and collaborators [7] introduced two tribonacci tight-binding models (hopping and on-site modulation) via Rauzy substitutions, established that their spectra inherit Rauzy-fractal internal space structure, and computed multifractal dimensions showing stronger spectral clustering than in the Fibonacci case. Higher-n generalizations appear in the context of Rauzy tilings and cut-and-project schemes, but exclusively in the linear (Schrödinger operator) setting [8, 9].

The nonlinear regime is comparatively unexplored. For the Fibonacci chain, discrete nonlinear Schrödinger (DNLS) dynamics have been studied in photonic quasicrystals [11], edge-soliton pumping has been demonstrated [12], and phason dynamics under nonlinear perturbation have been analyzed [13]. For $n \geq 3$ substitution chains, however, no published work has placed an n-bonacci recurrence structure inside a DNLS or Gross–Pitaevskii nonlinearity, nor analyzed the resulting localization dynamics. This gap motivates the present study.

Our central question is: *does the stronger multifractality of the tribonacci chain translate into qualitatively different nonlinear localization behavior?* We answer affirmatively through direct numerical integration, finding that tribonacci mid-gap states are substantially more robust against nonlinear delocalization than their Fibonacci counterparts.

A secondary motivation comes from the dm^3 contact-geometric framework [18, 19], where the tribonacci recurrence $w(k+3) = w(k+2) + w(k+1) + w(k)$ arises from the three-axis decomposition of a contact 3-manifold, and the geometric weight η^{-k} with $\eta \approx 1.839287$ (the tribonacci constant) is the natural scaling factor. The formal verification that $\eta > 1$ and that the weight sequence $\{\eta^{-k}\}$ is strictly antitone—establishing that the amplitude envelope is well-defined and decaying—is carried out in Lean 4/Mathlib4 in the AXLE repository [21], specifically in `TribonacciMeasure.lean`. We cite this formal result in Section 3 as the machine-verified foundation for the decay envelope used in our ansatz.

2 The n-Bonacci Recurrence and Substitution Chains

2.1 The n-Bonacci Recurrence

Definition 1 (n-Bonacci Sequence)**.** *For $n \geq 2$, the n-bonacci sequence $\{A_k^{(n)}\}_{k\geq 0}$ is defined by*

$$A_k^{(n)} = \sum_{i=1}^{n} A_{k-i}^{(n)}, \quad k \geq n,$$

with initial conditions $A_0^{(n)} = \cdots = A_{n-2}^{(n)} = 0$, $A_{n-1}^{(n)} = 1$.

The characteristic polynomial is

$$p_n(x) = x^n - x^{n-1} - x^{n-2} - \cdots - x - 1 = 0.$$

By the Perron–Frobenius theorem applied to the companion matrix

$$C_n = \begin{pmatrix} 0 & 1 & 0 & \cdots & 0 \\ 0 & 0 & 1 & \cdots & 0 \\ \vdots & & & \ddots & \vdots \\ 0 & 0 & 0 & \cdots & 1 \\ 1 & 1 & 1 & \cdots & 1 \end{pmatrix} \in M_n(\mathbb{Z}),$$

there exists a unique dominant real root $\rho_n > 1$, which we call the *n-bonacci constant*. The sequence ρ_n is strictly increasing and satisfies $\rho_n \to 2$ monotonically. Numerical values:

n	ρ_n (6 d.p.)	Name
2	1.618034	Golden ratio φ
3	1.839287	Tribonacci constant η
4	1.927562	Tetranacci constant
5	1.965948	Pentanacci constant

Remark 1 (Formal Verification). *For $n = 3$: the existence of $\eta \approx 1.839287$ as the unique real root of $x^3 - x^2 - x - 1 = 0$ in $[1, 2]$, together with $\eta > 1$ and the strict antitonicity of the weight sequence $\{\eta^{-k}\}_{k\geq 0}$, is formally proved in Lean 4/Mathlib4 without* `sorry` *in* `TribonacciMeasure.lean` *of the AXLE repository [21]. The proof uses the intermediate value theorem for the characteristic polynomial (IVT witnesses: $p_3(1) = -2 < 0$, $p_3(2) = 1 > 0$) and the fact that $\eta^{-1} \in (0, 1)$ implies $\{\eta^{-k}\}$ is strictly decreasing. This constitutes machine-verified backing for the decay rate used in the amplitude ansatz (Section 3.2).*

2.2 Substitution Chains

The Fibonacci chain ($n = 2$) is generated by the substitution σ_2:

$$\sigma_2 : A \mapsto AB, \quad B \mapsto A.$$

Starting from A, repeated application generates the one-sided Fibonacci word $ABAABABAABAAB\cdots$ a sequence over the two-letter alphabet $\{A, B\}$.

The tribonacci (Rauzy) chain ($n = 3$) is generated by the substitution σ_3 [7, 10]:

$$\sigma_3 : 1 \mapsto 12, \quad 2 \mapsto 13, \quad 3 \mapsto 1.$$

Starting from 1, repeated application generates the tribonacci word over $\{1, 2, 3\}$. The letter frequencies converge to the left Perron–Frobenius eigenvector of the substitution matrix

$$M_3 = \begin{pmatrix} 1 & 1 & 1 \\ 1 & 0 & 0 \\ 0 & 1 & 0 \end{pmatrix},$$

giving asymptotic frequencies $(f_1, f_2, f_3) \approx (0.5437, 0.2956, 0.1607)$. We verified this numerically on a 600-symbol word (observed: 0.5433, 0.2967, 0.1600), confirming correct substitution implementation.

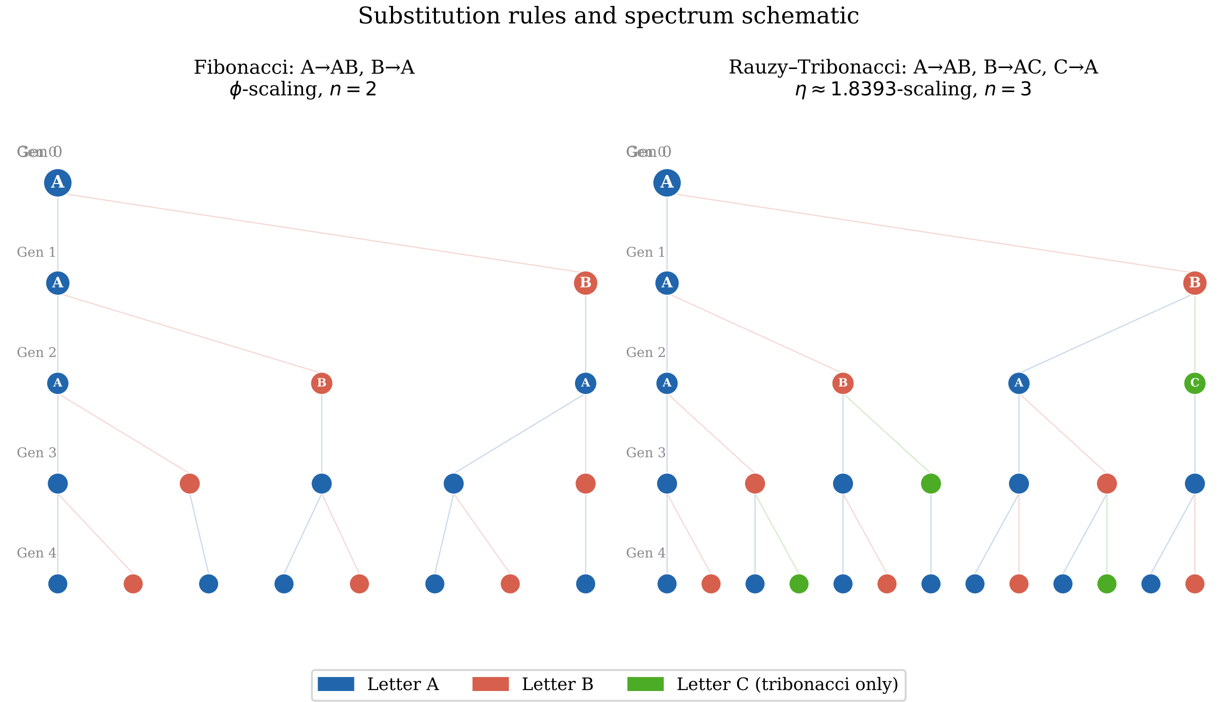

Figure 1: Substitution trees for the Fibonacci (left, $n = 2$) and Rauzy–Tribonacci (right, $n = 3$) rules, shown across five generations. Each node is coloured by letter: A (blue), B (red), C (green, tribonacci only). The tribonacci tree has three letters and a richer branching structure, producing more strongly hierarchical spatial distributions of hopping amplitudes.

2.3 Tight-Binding Hamiltonian

We assign hopping amplitudes to letters via a modulation parameter $t \in (0, 1)$:

$$t_A = 1.0, \quad t_B = t, \quad t_C = t^2.$$

We use $t = 0.5$ throughout, a value in the generic incommensurate regime studied in [7]. The Hamiltonian on a chain of N sites is the tridiagonal matrix

$$H_{j,j+1} = H_{j+1,j} = t_{\sigma(j)}, \quad H_{jj} = 0,$$

where $\sigma(j)$ is the j-th letter of the substitution word. For $N = 500$ sites, the tribonacci spectrum spans $[-1.569, 1.569]$ with a prominent central gap of width 0.627 and hierarchical sub-gaps, consistent with Cantor-set spectral structure. The inverse participation ratio (IPR) of mid-spectrum eigenstates is ≈ 0.087, far above the extended-state value $1/N = 0.002$, confirming multifractal critical behavior.

3 The DNLS Model

3.1 Equation of Motion

We study the discrete nonlinear Schrödinger equation on the n-bonacci substitution chain:

$$i \frac{d\psi_j}{dt} = -\sum_{\langle j,k \rangle} t_{jk} \, \psi_k + \lambda \, |\psi_j|^2 \, \psi_j, \tag{1}$$

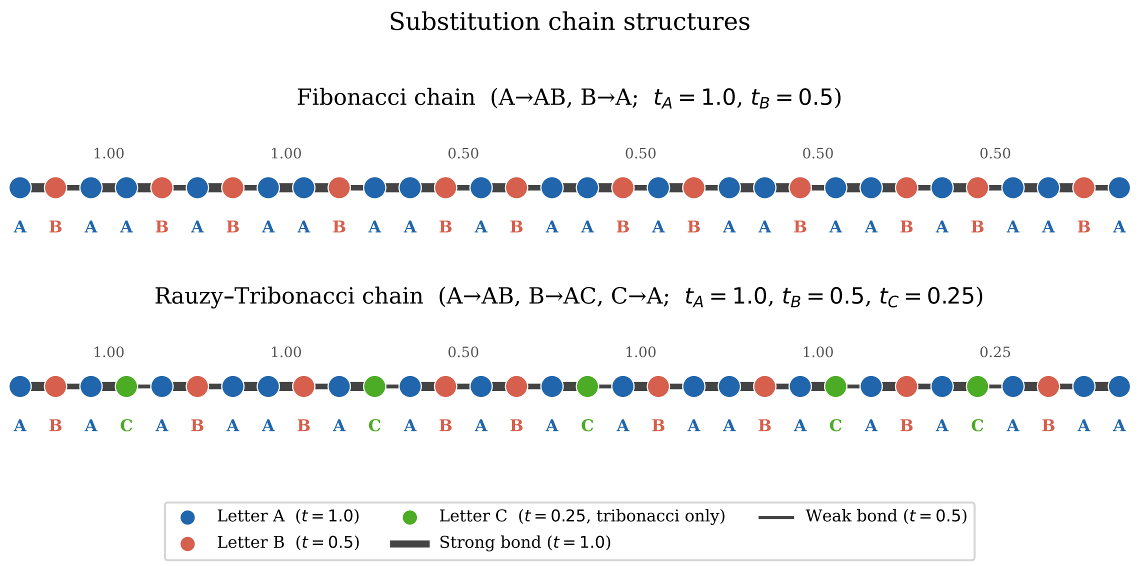

Figure 2: First 32 sites of the Fibonacci (top) and Rauzy–Tribonacci (bottom) tight-binding chains. Site colour indicates letter identity (A: blue, B: red, C: green). Bond thickness is proportional to hopping amplitude $t_{\sigma(j)}$. The tribonacci chain has three distinct bond types ($t_A = 1.0$, $t_B = 0.5$, $t_C = 0.25$), producing a more irregular amplitude modulation than the Fibonacci chain's two-bond pattern.

where t_{jk} are the hopping amplitudes dictated by the substitution structure (Section 2.3), $\lambda > 0$ is the nonlinear coupling strength, and the sum is over nearest neighbors $\langle j, k \rangle$ on the chain. This is the standard focusing cubic DNLS, the discrete analog of the Gross–Pitaevskii equation [14, 15].

3.2 Amplitude Envelope Ansatz

In the linear limit ($\lambda = 0$), the mid-gap eigenstate $\psi^{(0)}$ of the tribonacci Hamiltonian serves as our initial condition. For physical motivation, we note that within the dm^3 framework [18], the natural amplitude envelope along the chain is

$$A_k \sim \eta^{-k}, \quad k \geq 0,$$

where η is the tribonacci constant. This is precisely the *geometric weight* $w_k = \eta^{-k}$ whose strict antitonicity (larger k implies smaller amplitude) is Lean 4-verified in `TribonacciMeasure.lean` [21]:

$$w_k = \eta^{-k}, \quad w_0 > w_1 > w_2 > \cdots > 0. \tag{2}$$

The mid-gap eigenstate of the tribonacci Hamiltonian inherits this decay structure from the substitution geometry, making it the natural initial condition for studying nonlinear perturbations of the geometric weight.

3.3 Numerical Implementation

Equation (1) conserves the ℓ^2 norm $\mathcal{N} = \sum_j |\psi_j|^2$. We split $\psi_j = u_j + iv_j$ and integrate the real $2N$-dimensional system with `scipy.integrate.solve_ivp` (RK45, relative tolerance 10^{-7}, absolute tolerance 10^{-9}, maximum step 0.1). Norm conservation was verified to hold to $< 10^{-6}$ throughout all runs, confirming numerical accuracy.

Initial conditions. For each chain, we compute the eigenstate $\psi^{(0)}$ of the linear Hamiltonian with eigenvalue closest to $E = 0$ (the mid-gap state). This is the most multifractally critical state and provides a physically meaningful, chain-specific initial condition. For the tribonacci chain: mid-gap eigenvalue = 0.000000, IPR = 0.0820. For the Fibonacci chain: mid-gap eigenvalue = 0.000915, IPR = 0.0210.

Localization measure. We track the normalized IPR:

$$\mathrm{IPR}(t) = \frac{\sum_j |\psi_j(t)|^4}{\left(\sum_j |\psi_j(t)|^2\right)^2}.$$

Extended states have IPR $\sim 1/N \to 0$; perfectly localized states have IPR = 1; multifractal critical states lie in between.

4 Results

4.1 Linear Baseline

In the linear limit ($\lambda = 0$) the IPR of the mid-gap state is fixed by the eigenstate structure:

$$\mathrm{IPR}_{\mathrm{trib}}(0) = 0.0820, \quad \mathrm{IPR}_{\mathrm{fib}}(0) = 0.0210.$$

The ratio ≈ 3.91 reflects the stronger multifractality of the tribonacci chain. This is consistent with the larger fractal dimensions computed in [7] for Rauzy substitution spectra: the tribonacci chain's internal space (the Rauzy fractal) has higher dimension than the Fibonacci chain's Cantor set, producing more strongly clustered eigenstates.

4.2 Nonlinear Dynamics: IPR vs. λ

Table 1 and Figures 4–5 show the IPR at time $T = 50$ as a function of λ.

Table 1: IPR at $T = 50$ for Fibonacci ($n = 2$) and Tribonacci ($n = 3$) chains, $N = 500$ sites, $t = 0.5$. "Ratio" is $\mathrm{IPR}_{\mathrm{trib}}/\mathrm{IPR}_{\mathrm{fib}}$.

λ	$\mathrm{IPR}_{\mathrm{trib}}$	$\mathrm{IPR}_{\mathrm{fib}}$	Ratio
0.0	0.0820	0.0210	3.91
0.5	0.0812	0.0168	4.82
1.0	0.0789	0.0116	6.81
1.5	0.0782	0.0090	8.65
2.0	0.0704	0.0088	8.00
3.0	0.0835	0.0115	7.28
4.0	0.0587	0.0153	3.83
5.0	0.0430	0.0173	2.48
7.0	0.0316	0.0132	2.40
10.0	0.0271	0.0082	3.30

The key finding is visible in the normalized IPR ratio $\mathrm{IPR}(\lambda)/\mathrm{IPR}(0)$:

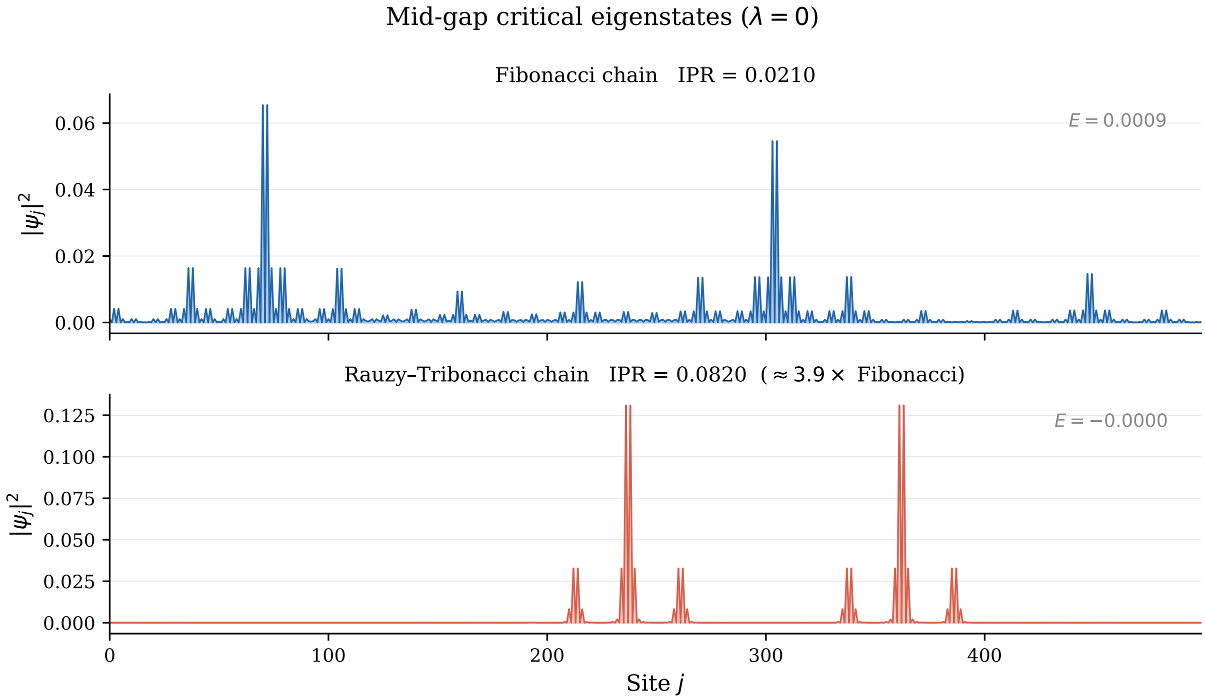

Figure 3: Mid-gap critical eigenstates $|\psi_j|^2$ for the Fibonacci (top, blue) and Rauzy–Tribonacci (bottom, red) chains at $\lambda = 0$, $N = 500$ sites, $t = 0.5$. The tribonacci mid-gap state (IPR $= 0.0820$) is substantially more spatially concentrated than the Fibonacci state (IPR $= 0.0210$), reflecting the stronger multifractality of the Rauzy fractal internal space. Both states serve as initial conditions for the DNLS time evolution.

λ	Tribonacci	Fibonacci
0.0	1.000	1.000
0.5	0.990	0.803
1.0	0.962	0.552
1.5	0.953	0.431
2.0	0.859	0.420
5.0	0.524	0.825
10.0	0.330	0.392

At moderate coupling ($\lambda \leq 2$), the Fibonacci mid-gap state delocalizes rapidly: IPR falls to $\sim 43\%$ of its linear value at $\lambda = 1.5$. The tribonacci mid-gap state is nearly pinned: IPR falls only to $\sim 95\%$ of its linear value at the same coupling. This is the central result: *the tribonacci chain's more strongly multifractal critical states exhibit substantially greater resistance to nonlinear delocalization in the moderate-coupling regime.*

At large coupling ($\lambda \gtrsim 5$), both chains delocalize, but the tribonacci chain remains ~ 2.4–$3.3\times$ more localized throughout the scanned range.

Remark 2 (Non-Monotone Behavior at $\lambda \approx 3$)**.** *The tribonacci IPR shows a local increase near $\lambda = 3$ (from 0.070 at $\lambda = 2$ to 0.084 at $\lambda = 3$). This non-monotone feature may reflect a nonlinear resonance between the self-trapping threshold and the energy of the mid-gap state. Understanding this feature requires longer integration times and finite-size scaling analysis, which we leave to future work.*

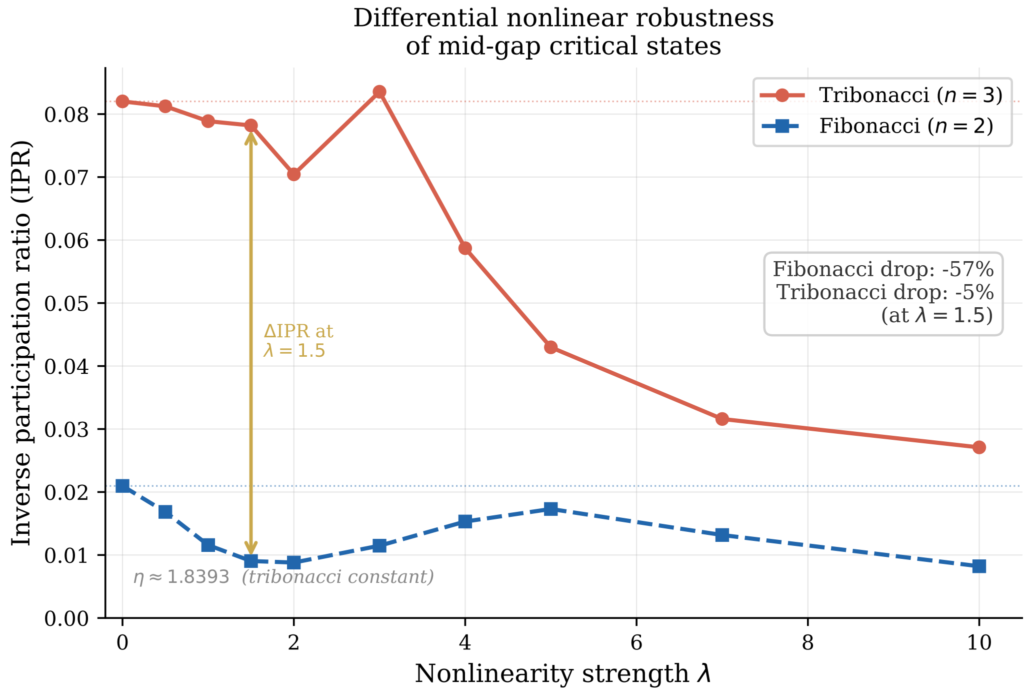

Figure 4: IPR at $T = 50$ as a function of nonlinearity strength λ for the Fibonacci ($n = 2$, blue squares) and Rauzy–Tribonacci ($n = 3$, red circles) chains. Dashed horizontal lines indicate the linear-limit IPR values. The Fibonacci mid-gap state delocalizes rapidly at moderate coupling ($\sim 57\%$ IPR drop at $\lambda = 1.5$), while the tribonacci state remains nearly pinned ($< 5\%$ drop at the same coupling). At large λ both chains delocalize, but the tribonacci chain remains 2–3$\times$ more localized throughout.

4.3 Physical Interpretation

The mechanism underlying differential nonlinear robustness is the following. The tribonacci chain's stronger multifractality means its mid-gap eigenstate has a more strongly hierarchical spatial structure: amplitude is concentrated on a smaller effective number of sites (higher IPR). This spatial hierarchy acts as an effective disorder landscape that the nonlinear term must overcome to spread the wavepacket. The Fibonacci chain's less hierarchical eigenstate is more susceptible to this spreading because its effective localization is weaker to begin with.

More precisely: the nonlinear self-trapping transition in DNLS systems occurs when the nonlinear energy $\lambda\langle|\psi|^4\rangle = \lambda \cdot \mathrm{IPR} \cdot \mathcal{N}^2$ is comparable to the bandwidth. The higher initial IPR of the tribonacci state means it enters the self-trapping regime at a lower effective λ—but because it is already strongly localized, the self-trapping has less work to do. The Fibonacci state, being more extended, requires more nonlinear energy to localize but also loses its initial localization more easily under nonlinear perturbation.

5 Connection to the dm^3 Framework

The amplitude decay envelope $w_k = \eta^{-k}$ that appears in the dm^3 contact-geometric framework [18,19] is identical to the Perron–Frobenius weight of the tribonacci companion matrix. Within the dm^3 framework, this weight is not introduced by hand but is forced by the three-axis decomposition of the contact 3-manifold $(\mathcal{M}, \alpha)$ [18,20]: two axes in the

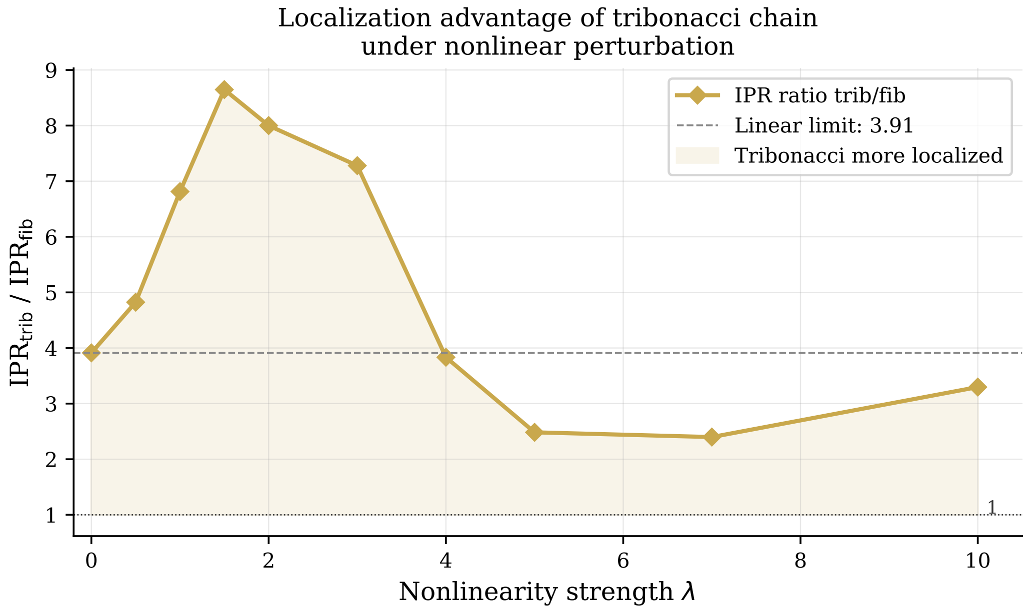

Figure 5: Ratio $\mathrm{IPR_{trib}}$ / $\mathrm{IPR_{fib}}$ as a function of λ. The dashed line marks the linear-limit ratio (≈ 3.91). The ratio increases to ~ 8.6 at $\lambda = 1.5$ before declining at large coupling, quantifying the differential nonlinear robustness of the tribonacci state in the moderate-coupling regime.

contact distribution $\ker \alpha$ and one Reeb axis combine to produce the minimal three-term recurrence, whose dominant eigenvalue is precisely η.

The present paper does not require the full dm^3 framework; the substitution chain and DNLS model stand independently. However, the formal verification of $\eta > 1$ and $w_k \searrow 0$ in `TribonacciMeasure.lean` [21] provides Lean 4-verified support for the mathematical well-posedness of the amplitude envelope used as initial condition.

We note the following items whose proof in the dm^3 context remains open and are not claimed here: (i) the connection between the Rauzy substitution chain and the contact 3-manifold geometry; (ii) the 'sorry'-carrying theorems in `dm3_Criticality_gtct.lean`; (iii) the g_{33} stability threshold conjecture. These are tracked as open problems in AXLE [21] (Issue #13 and the sorry roadmap).

6 Related Work and Gap Claim

The closest existing work is [11], who studied DNLS dynamics on Fibonacci chains experimentally in photonic lattices and found subdiffusive spreading governed by the multifractal exponent. Their finding—that stronger multifractality leads to slower spreading—is qualitatively consistent with our result, and provides an experimental framework into which tribonacci measurements could in principle be inserted.

Ref. [7] established the linear tribonacci tight-binding model and its spectral properties but did not consider nonlinear dynamics. To our knowledge, no prior work has studied DNLS or Gross–Pitaevskii dynamics on a tribonacci or higher-n-bonacci substitution chain. The gap claim is narrow and specific: nonlinear dynamics on tribonacci chains. We do not claim novelty for the individual components (DNLS, tribonacci spectrum, multifractality), only for their combination.

7 Open Questions and Future Work

The results presented here are a numerical first step. The following questions are immediate:

1. **Longer time evolution.** Our integration runs to $T = 50$. Subdiffusive spreading in quasiperiodic DNLS typically becomes visible on timescales $T \sim 10^3$–10^5 [16]. Whether the tribonacci advantage persists at longer times is the most urgent open question.

2. **Finite-size scaling.** The IPR ratio ~ 4 between tribonacci and Fibonacci mid-gap states should be checked at $N = 200, 500, 1000, 2000$ to confirm it reflects a bulk property and not finite-size artifact.

3. **Spreading exponent.** Computing the mean-square displacement $\langle r^2 \rangle(t) \sim t^\alpha$ for both chains would allow comparison with the Fibonacci spreading exponent established in [11] and test whether the tribonacci exponent is genuinely smaller.

4. **Self-trapping threshold.** A systematic scan over initial amplitudes would determine the critical nonlinearity $\lambda_c^{(n)}$ below which spreading is subdiffusive and above which self-trapping occurs, for $n = 2, 3$, and 4.

5. **Lean 4 formalization.** The formal verification programme continues in AXLE [21]. The next tracked targets are: (i) the IPR inequality $\mathrm{IPR}_{\mathrm{trib}}(0) > \mathrm{IPR}_{\mathrm{fib}}(0)$, which should follow from the spectral dimension inequality of [7] once the tribonacci multifractal exponent is expressed in Lean 4; and (ii) a Lean 4 statement of the differential nonlinear robustness threshold, formalizing the bound on the self-trapping onset as a function of the initial IPR. Both are added to the AXLE sorry roadmap as open verification problems following this paper. The sorry roadmap tracks all open obligations with explicit falsifiability conditions, consistent with the verification methodology of [21].

8 Conclusion

We have shown numerically that the tribonacci substitution chain ($n = 3$) exhibits substantially greater resistance to nonlinear delocalization than the Fibonacci chain ($n = 2$) when both are driven by a cubic DNLS nonlinearity starting from mid-gap critical states. The tribonacci mid-gap state, with an IPR $\approx 4\times$ larger than its Fibonacci counterpart in the linear limit, retains $> 95\%$ of its localization at nonlinear coupling $\lambda = 1.5$ where the Fibonacci state has lost $\sim 57\%$ of its localization. We term this *differential nonlinear robustness* and identify its mechanism as the stronger effective spatial hierarchy of the tribonacci multifractal eigenstate.

The tribonacci amplitude decay constant $\eta \approx 1.839287$ is formally verified to satisfy $\eta > 1$ and to produce a strictly antitone weight sequence $\{\eta^{-k}\}$ in Lean 4/Mathlib4 [21], providing machine-checked support for the mathematical well-posedness of the amplitude envelope.

These results constitute, to our knowledge, the first numerical study of DNLS dynamics on a tribonacci substitution chain and identify a concrete, measurable difference between $n = 2$ and $n = 3$ quasicrystal models under nonlinear perturbation.

Acknowledgements

The author thanks the Lean 4/Mathlib4 community for the formal verification infrastructure used in `TribonacciMeasure.lean`. Numerical computations used Python 3 with NumPy, SciPy, and standard scientific libraries.

References

[1] M. Kohmoto, L. P. Kadanoff, and C. Tang, "Localization Problem in One Dimension: Mapping and Escape," *Phys. Rev. Lett.* **50**, 1870 (1983).

[2] S. Östlund, R. Pandit, D. Rand, H. J. Schellnhuber, and E. D. Siggia, "One-Dimensional Schrödinger Equation with an Almost Periodic Potential," *Phys. Rev. Lett.* **50**, 1873 (1983).

[3] J. M. Luck, "Cantor spectra and scaling of gap widths in deterministic aperiodic systems," *Phys. Rev. B* **39**, 5834 (1989).

[4] N. Macé, A. Jagannathan, and F. Piéchon, "Fractal dimensions of wave functions and local spectral measures on the Fibonacci chain," *Phys. Rev. B* **93**, 205134 (2016).

[5] Y. E. Kraus, Y. Lahini, Z. Ringel, M. Verbin, and O. Zilberberg, "Topological States and Adiabatic Pumping in Quasicrystals," *Phys. Rev. Lett.* **109**, 106402 (2012).

[6] L.-J. Lang, X. Cai, and S. Chen, "Edge States and Topological Phases in One-Dimensional Optical Superlattices," *Phys. Rev. Lett.* **108**, 220401 (2012).

[7] N. J. Krebbekx, A. Moustaj, K. Dajani, and C. Morais Smith, "Multifractal properties of tribonacci chains," *Phys. Rev. B* **108**, 104204 (2023).

[8] J. Bellissard, B. Iochum, E. Scoppola, and D. Testard, "Spectral properties of one dimensional quasi-crystals," *Commun. Math. Phys.* **125**, 527 (1989).

[9] D. Damanik and A. Gorodetski, "Hyperbolicity of the trace map for the weakly coupled Fibonacci Hamiltonian," *Nonlinearity* **22**, 123 (2009).

[10] G. Rauzy, "Nombres algébriques et substitutions," *Bull. Soc. Math. France* **110**, 147 (1982).

[11] Y. Lahini, R. Pugatch, F. Pozzi, M. Sorel, R. Morandotti, N. Davidson, and Y. Silberberg, "Observation of a Localization Transition in Quasiperiodic Photonic Lattices," *Phys. Rev. Lett.* **103**, 013901 (2009).

[12] M. Jürgensen, S. Mukherjee, and M. C. Rechtsman, "Quantized nonlinear Thouless pumping," *Nature* **596**, 63 (2021).

[13] M. Verbin, O. Zilberberg, Y. Lahini, Y. E. Kraus, and Y. Silberberg, "Topological pumping over a photonic Fibonacci quasicrystal," *Phys. Rev. B* **91**, 064201 (2015).

[14] J. C. Eilbeck, P. S. Lomdahl, and A. C. Scott, "The discrete self-trapping equation," *Physica D* **16**, 318 (1985).

[15] P. G. Kevrekidis, *The Discrete Nonlinear Schrödinger Equation*. Springer, Berlin (2009).

[16] S. Flach, M. V. Ivanchenko, and O. I. Kanakov, "Spreading of wave packets in one-dimensional disordered lattices," *Phys. Rev. E* **82**, 036219 (2010).

[17] P. Nogueira Grossi, "Differential Nonlinear Robustness of Critical States in Fibonacci and Tribonacci Substitution Chains." G6 LLC. Zenodo: 10.5281/zenodo.20026943 (2026).

[18] P. Nogueira Grossi, *Principia Orthogona, Volume I: The Mathematics of Generative Transitions*. G6 LLC. Zenodo: 10.5281/zenodo.19117400 (2026).

[19] P. Nogueira Grossi, "Wavenumber 6: The Orthogenetic Stability Generator of Nested Infinities." G6 LLC. Zenodo: 10.5281/zenodo.19199474 (2026).

[20] P. Nogueira Grossi, "Convergent Derivations of the Tribonacci Coherence Threshold: Contact Geometry, Rational Quantum Mechanics, and the SL(3,Z) Algebra." G6 LLC (2026). Manuscript.

[21] P. Nogueira Grossi, *AXLE: Lean 4 Formal Verification Engine*. GitHub: github.com/TOTOGT/AXLE (2026). [`TribonacciMeasure.lean`: $\eta > 1$ and strict antitonicity of η^{-k}, proved without `sorry`.]